Supporting Information for "Complex Relaxation of Trapped Spin-States in Spin Crossover Materials"

M. Nadeem and Ben J. Powell*

School of Mathematics and Physics, The University of Queensland, Brisbane, Queensland, 4072, Australia

E-mail: powell@physics.uq.edu.au

Model

To study the collective dynamics of trapped spin-states, we recently developed a semi-classical approach to model spin-crossover materials.[1] In this method, the single-molecular quantum chemistry, essential to describe the photoexcitation and relaxation behaviors, is combined with classical elastic interactions between molecules. We consider d^6 transition metal complexes with octahedral inner coordination spheres – archetypal spin-crossover compounds. For the effective theory, we include the three lowest energy states within the crystal field theory: $^1A_1$, $^3T_1$ and $^5T_2$, which we label LS, HS, and IS respectively. Many electron energies are parameterized with the Racah parameter, B, and ligand-field, Dq.[2] The spin-orbit coupling, ζ, allows the transition between the HS and LS states, mediated by the high energy IS state. Moreover, ζ introduces zero-field splittings between the 15-fold degenerate HS states.[1] We explicitly include the symmetric breathing coordinate of the metal-ligand octahedron, which is strongly coupled with the spin-states.[3] A harmonic potential, with

a spring constant κ_{A_1}, is assumed for the symmetric molecular vibration. The minima of potential energies are chosen to occur at $Q = -\delta$ for LS, $Q = 0$ for IS and $Q + \delta$ for HS. The minimum energy of each state is obtained from crystal field theory (i.e., the d^6 Tanabe-Sugano diagram).

Typically, the LS and HS manifolds are much lower in energy than the IS state. Treating the spin-orbit coupling perturbatively, we integrate out high-energy IS state and diagonalize the resulting low-energy manifold of the system to obtain effective potential surfaces (PES); plotted, for typical parameter values (Table S1), in Fig. 1a. This, results[1] in a double well PES (red) with mixed LS, IS, and HS character, and 14 pure HS states (gray) split into three levels with degeneracies 3, 5 and 6. Double well potentials have been previously proposed as models of SCO materials[4,5] on purely phenomenological grounds. However, such models neglect the pure HS levels that are a vital part of our theory and lack the connection to microscopic quantum theory that we make.

In SCO materials, elastic interactions[6] arise from a variety of competing intermolecular interactions; this can include covalent bonds in frameworks but also includes weak interactions. Indeed, in molecular crystals weak interactions hold the crystal together and are responsible for elasticity. Weak interactions have also been shown to play a crucial role in deriving collective SCO behaviors even in framework materials.[7–11] Generally, the interaction between a pair of SCO molecules will be anharmonic. In equilibrium structures, intermolecular forces are not individually minimized – rather the total free energy is minimized. This induces elastic frustration into structures. Nevertheless, arbitrary intermolecular interactions can be represented as harmonic potentials at the lowest non-trivial order, figure S1; however, elastic frustration leads to some force constants being negative.[11,12] This representation of intermolecular interactions as a network of springs allowed the discovery of structure-property relationships between crystal structures and the intermediate spin-state orders that appear during thermal SCO in framework materials.[11] These predictions are consistent with all experimental observations to date. This emphasizes that, even in framework materials, be-

yond the nearest neighbor, weak interactions play a crucial role in understanding collective SCO phenomena and, therefore, cannot be neglected. Therefore, in this work, we include elastic interactions up to the third nearest neighbors and a harmonic potential for angular distortions.

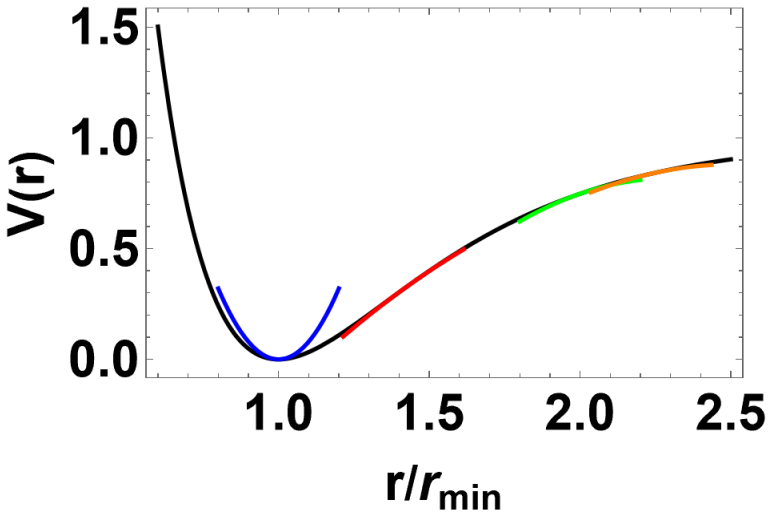

Figure S1: Spring constants as effective potentials. Here we compare interactions governed by a Moorse potential (black) with approximate spring-like (i.e., harmonic) potentials at first (blue), second (red), third (green), and forth (orange) nearest neighbour distances, taking nearest neighbours to be at the minimum of the potential. Note that except for nearest neighbors the spring constants are negative and the third nearest neighbor spring constant is larger than the second nearest neighbor spring constant. Explicitly $\kappa_2/\kappa_1 = -0.06$, $\kappa_3/\kappa_1 = -0.10$, and $\kappa_2/\kappa_1 = -0.07$. A similar analysis holds for other chemically reasonable potentials, e.g., the Lennard-Jones potential.[11]

We place N such spin-crossover centers on a square lattice with classical elastic interactions between neighbors, as sketched in Fig. 1. The model Hamiltonian is thus

$$H = \sum_{i}^{N} \left[\frac{\mathbf{p}_i^2}{2m} + \frac{\mathbf{P}_i^2}{2M} + V_\nu(Q_i) + \sum_{<i,j>_n} U_n(Q_i, Q_j, \mathbf{r}_i, \mathbf{r}_j) + \sum_{<i,j,k>_1} U_\theta(\mathbf{r}_i, \mathbf{r}_j, \mathbf{r}_k) \right], \quad \text{(S1)}$$

where $V_\nu(Q_i)$ is an internal potential energy surface, $\mathbf{r}_i$ is position of the ith molecule, with mass m and conjugate momentum $\mathbf{p}_i$, and M is mass associated with the momentum, P, of the breathing coordinate, Q. The elastic interaction between two nth nearest neighbors is

given by

$$U_n = \frac{\kappa_n}{2}\left(|\mathbf{r}_i - \mathbf{r}_j| - \mu_n(2\bar{d} + Q_i + Q_j)\right)^2, \tag{S2}$$

where $\mu_1 = 1$, $\mu_2 = \sqrt{2}$, and $\mu_3 = 2$, and the harmonic potential associated with angular distortions is

$$U_\theta = \frac{\kappa_\theta}{2}\sin^2\left(\frac{\pi}{2} - \theta\right), \tag{S3}$$

where θ is the angle between the nearest neighbor bonds, Fig. 1.

Typical parameters for SCO materials have previously been estimated.[1] Except as explicitly noted these parameters are used for all calculations in the paper and are listed in table S1. We solve the model on a 30×30 lattice using molecular dynamics . As the model has $30 \times 30 \times 3 = 2700$ degrees of freedom, explicit, direct mapping of free energy is not possible.

Table S1: "Typical" values of the parameters in the model, based on previous analysis of experiments on SCO materials.[1] Except as explicitly noted, these parameters are used in all calculations in this paper.

Parameter	**Value**
B	100 meV
C/B	4.81
Dq/B	2.039
ζ	14.6 meV
κ_{A_1}	10.34 eV/Å^2
δ	0.1 Å
ω_{HS}	5×10^{13} s^{-1}
ω_{LS}	8×10^{13} s^{-1}
κ_1	0.86 eV/Å^2
κ_2	0.2 κ_1
κ_3	0
κ_θ	0

Molecular Dynamics Methods

We simulate the system with molecular dynamics (MD) at a constant temperature, a constant pressure and a constant number of molecules on a 30×30 square lattice, using the Nose-Hoover thermostat and the Anderson barostat.[13] Separate thermostats are applied for lattice and internal coordinates to circumvent the flying ice cube problem.[14] We assume barrierless transitions within HS states, and the thermal occupancy of the internal PESs is determined by applying 20 Metropolis Monte Carlo steps after every 50 MD steps.

To simulate isothermal kinetic experiments, we initialize the simulation in an all-HS state at the set temperature, then we let the ensemble evolve in time at constant temperature for 2.5×10^6 MD steps. The change in the magnetic response, χT, of a sample with time and temperature is calculated, where χ is magnetic susceptibility. In the thermally accelerated approach, light is used to prepared a sample in a trapped phase at 10 K, once the light is switched off, the sample is heated until it decays to LS.[15] To simulate this, we initialize at HS and let the molecular dynamics evolve to 5.5×10^5 MS steps at a set temperature and increase the temperature by 0.5 K. Experimentally, HS$\rightarrow$LS relaxation timescales vary widely: from extremely fast to many hours.[16–23] The microscopic variation of the model parameters allows us to set a small single molecular energy barrier to the trapped states (shown in Fig. 1a) without significantly changing the other physics of the problem. This allows us to probe the dynamics of these materials within computable timescales and without numerically accelerating the calculations.

For thermal SCO, the sample is initialized in the all-HS state at a high temperature, cooled down to 10 K, and then heated to the initial high temperature. For thermal SCO, the temperature is changed in 1.0 K intervals.

We calculate structure factor, $S(\boldsymbol{q}) = \langle I(\boldsymbol{q}) I^*(\boldsymbol{q}) \rangle$, where $\langle ... \rangle$ indicates ensemble averag-

ing,

$$I(\boldsymbol{q}) = \frac{1}{\sqrt{N}} \sum_{j}^{N} \left(e^{i\boldsymbol{q}.\boldsymbol{R}_j} + e^{i\boldsymbol{q}.(\boldsymbol{R}_j + (\bar{r}+Q_j)\hat{x})} + e^{i\boldsymbol{q}.(\boldsymbol{R}_j + (\bar{r}+Q_j)\hat{y})} + e^{i\boldsymbol{q}.(\boldsymbol{R}_j + (\bar{r}-Q_j)\hat{x})} + e^{i\boldsymbol{q}.(\boldsymbol{R}_j + (\bar{r}-Q_j)\hat{y})} \right), \tag{S4}$$

is Fourier transform of positions of the metals and ligands, and $\bar{r} = 2.0$ $\mathring{A}$ is the average of LS and HS metal-ligand bond length.[3] The positions of four ligands and one metal centre per spin-crossover complex are considered to calculate the 2D structure factor.

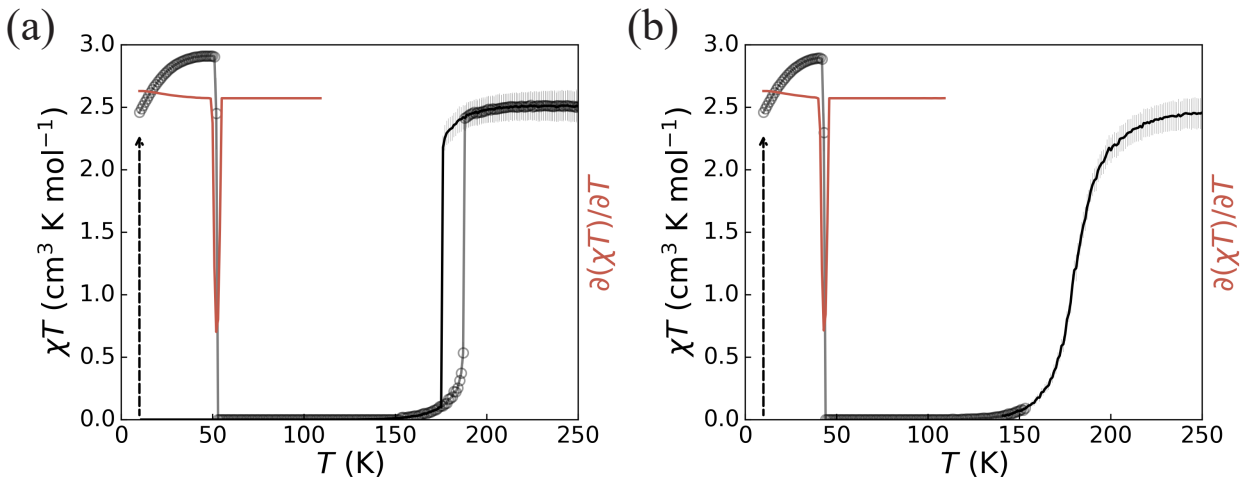

Figure S2: Cooperative thermally activated decay from the trapped HS state corresponding to Fig. 2. (a) Thermally accelerated relaxation of the trapped HS state (black circles) and the (first-order) thermal SCO transition (black lines), for the parameters given in Table S1. $\partial(\chi T)/\partial T$ (red line) has a negative peak at $T_{\mathrm{LIESST}} = 52$ K. (b) Decreasing the intermolecular interactions (here $\kappa_2 = 0.06\kappa_1$, versus $\kappa_2 = 0.2\kappa_1$ in (a)) drives the first order thermal SCO phase transition to a crossover and decreases T_{LIESST} to 43 K.

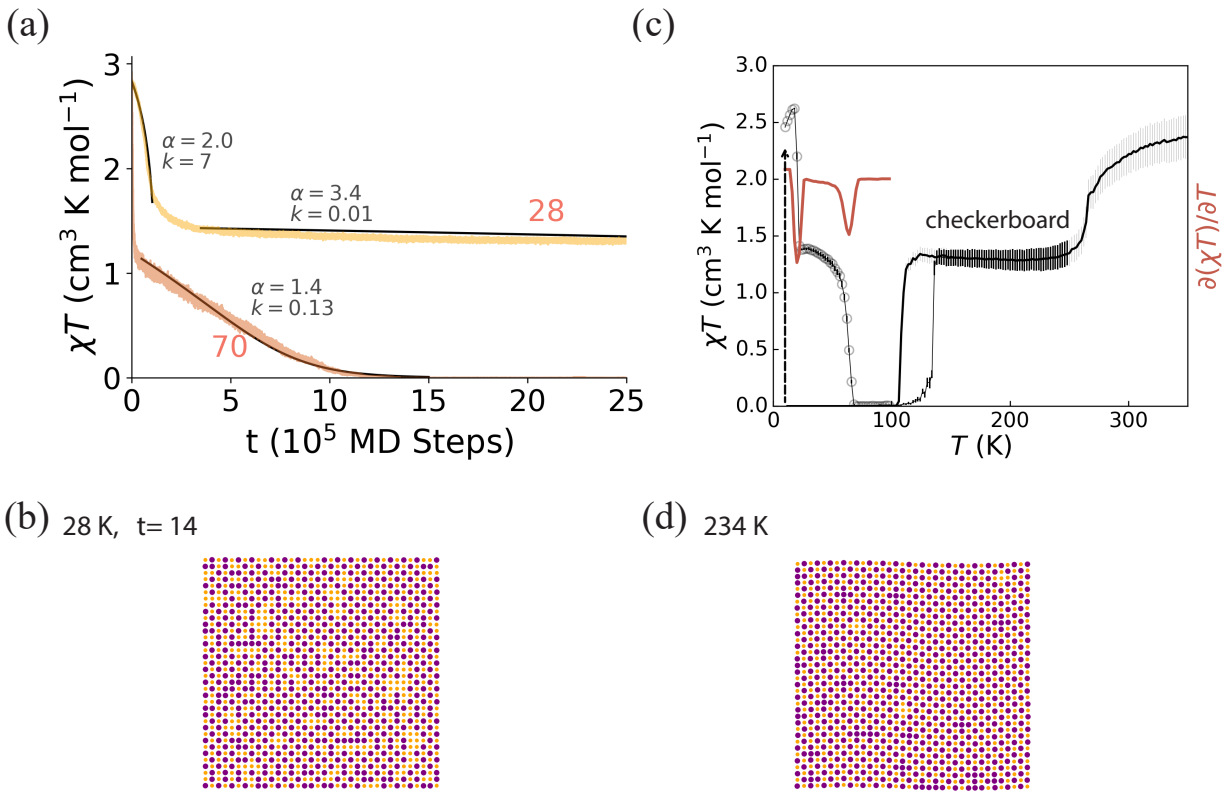

Figure S3: Two-step relaxation involving checkerboard intermediate spin-state order is similar to two-step relaxation with stripe intermediate order (Fig. 3). (a) Isothermal relaxation is sigmoidal for both steps (black lines). (b) A typical snapshot of the short-range checkerboard state that appears at the intermediate plateau during isothermal reactions. (c) The two-step thermal transition with a long-range ordered, symmetry-breaking, checkerboard phase in the intermediate plateau. Similarly, the thermally accelerated relaxation of the trapped HS state is two step. Thus, $\partial(\chi T)/\partial T$ has two negative peaks. (d) A typical spin-state configuration at the intermediate step during the cooling sweep of thermal SCO. Here $\kappa_2 = 0.15\kappa_1$, $\kappa_3 = -0.20\kappa_1$ and $Dq/B = 2.0503$.

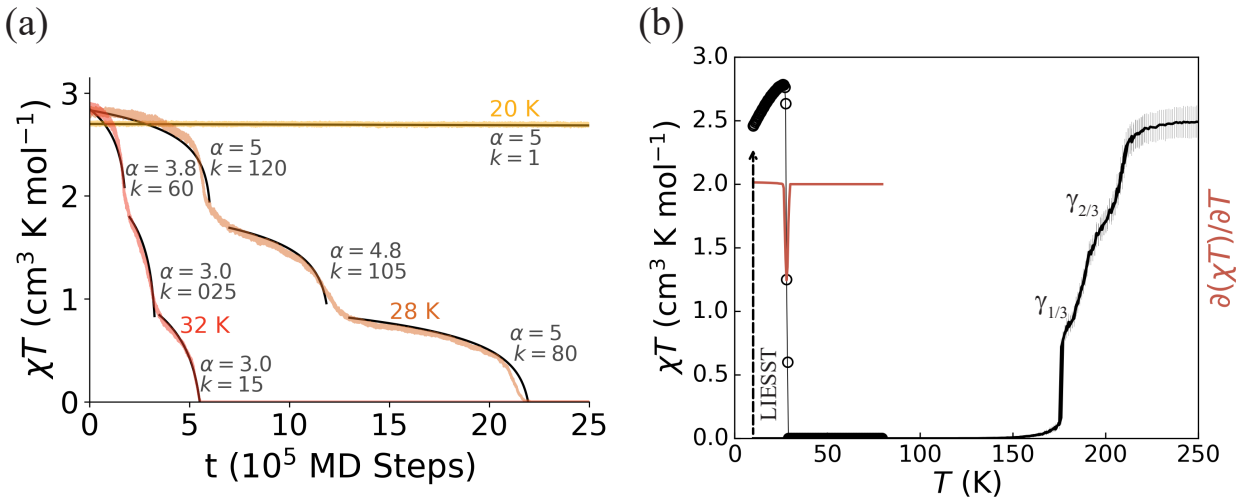

Figure S4: Complete, three-step relaxation involving two intermediate plateaus. Multiple steps are also found in the isothermal relaxation. Here $Dq/B = 2.0459$ $\kappa_1 = 1.55\text{eV/Å}^2$, $\kappa_2 = -0.21\kappa_1$, $\kappa_3 = 0.1\kappa_1$, and $\kappa_\theta = 0.56\kappa_1$.

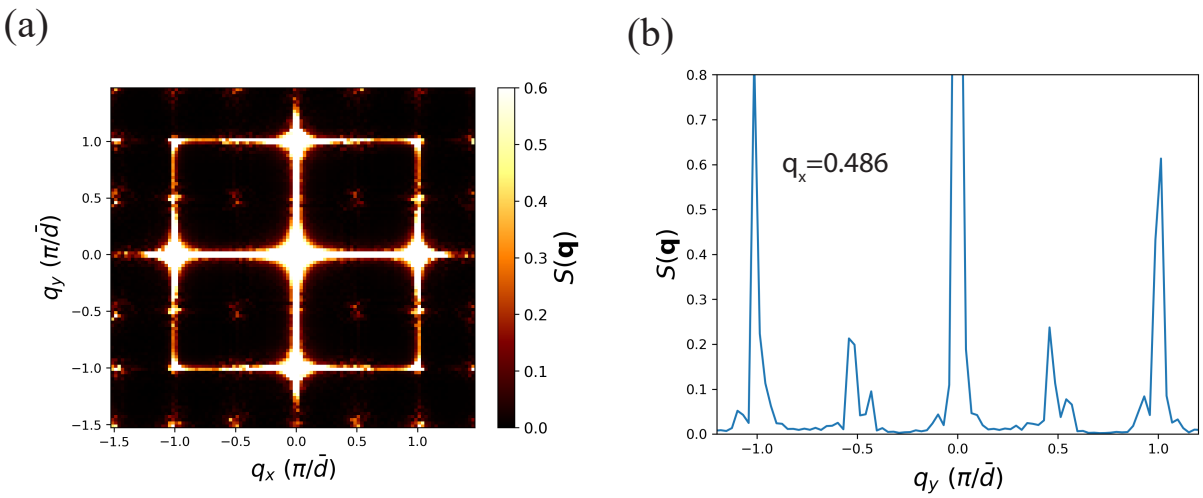

Figure S5: Time averaged structured factor, $S(\boldsymbol{q})$ (see Eq S4), of complex relaxation kinetics shows simultaneously existing peaks related to the stripe, checkerboard, $HS_{3/4}$ and $HS_{1/4}$ states. (a) Structure factor for isothermal relaxation at 40 K corresponding to the parameters used in Fig. 6a. The average $\langle S(\boldsymbol{q})\rangle$ is taken over five simulation runs and from 0 to 25×10^5 MD steps for each run. $2\bar{d}$ is the mean of the all-LS and all-HS unit cell lengths. For the all-HS and all-LS states, the unit cell is square and $S(\boldsymbol{q})$ has a single Bragg peak at the Brillion zone center $\boldsymbol{q} = (0,0)$. For stripe order, an additional peak appears in $S(\boldsymbol{q})$ at $\boldsymbol{q} = (0,\pi/2\bar{d})$ or $\boldsymbol{q} = (\pi/2\bar{d},0)$ for horizontally or vertically arranged stripes, respectively. For the checkerboard state, an additional peak appears at $\boldsymbol{q} = (\pi/2\bar{d},\pi/2\bar{d})$. $HS_{3/4}$ and $HS_{1/4}$ give additional peaks at $\boldsymbol{q} = (\pi/2\bar{d},0)$, $(0,\pi/2\bar{d})$ and $(\pi/2\bar{d},\pi/2\bar{d})$. $S(\boldsymbol{q})$ clearly shows additional peaks at all of these points, indicating that correlations are present for each of these orders. The inherent disorder and mismatch of unit cell lengths of different states broadens and splits the peaks, indicating that the order is short-range and short-lived. The splitting and broadening can be seen more clearly in (b), where we plot $S(\boldsymbol{q})$ for fixed $q_x = \pi/2\bar{d}$.

References

(1) Nadeem, M.; Cruddas, J.; Ruzzi, G.; Powell, B. J. Toward high-temperature light-induced spin-state trapping in spin-crossover materials: the interplay of collective and molecular effects. *J. Am. Chem. Soc.* **2022**, *144*, 9138–9148.

(2) Sugano, S.; Tanabe, Y.; Kamimura, H. *Multiplets of transition-metal ions in crystals*; Academic Press, 1970.

(3) Gütlich, P.; Goodwin, H. A. In *Spin crossover in transition metal compounds I*; Gütlich, P., Goodwin, H., Eds.; Springer Berlin Heidelberg: Berlin, Heidelberg, 2004; pp 1–47.

(4) Nishino, M.; Boukheddaden, K.; Konishi, Y.; Miyashita, S. Simple Two-Dimensional Model for the Elastic Origin of Cooperativity among Spin States of Spin-Crossover Complexes. *Phys. Rev. Lett.* **2007**, *98*, 247203.

(5) Nishino, M.; Boukheddaden, K.; Miyashita, S.; Varret, F. Dynamical property of nucleation in spin crossover depending on the system boundary. *Journal of Physics: Conference Series* **2009**, *148*, 012034.

(6) Batsanov, A. S. Weak interactions in crystals: old concepts, new developments. *Acta Crystallographica Section E: Crystallographic Communications* **2018**, *74*, 570–574.

(7) Liu, F.-L.; Tao, J. Hysteretic Two-Step Spin-Crossover Behavior in Two Two-Dimensional Hofmann-Type Coordination Polymers. *Chemistry–A European Journal* **2017**, *23*, 18252–18257.

(8) Sciortino, N. F.; Ragon, F.; Klein, Y. M.; Housecroft, C. E.; Davies, C. G.; Jameson, G. N.; Chastanet, G.; Neville, S. M. Guest-responsive elastic frustration "On–Off" switching in flexible, two-dimensional spin crossover frameworks. *Inorganic Chemistry* **2018**, *57*, 11068–11076.

(9) Clements, J. E.; Price, J. R.; Neville, S. M.; Kepert, C. J. Hysteretic Four-Step Spin Crossover within a Three-Dimensional Porous Hofmann-like Material. *Angewandte Chemie* **2016**, *128*, 15329–15333.

(10) Agustí, G.; Muñoz, M. C.; Gaspar, A. B.; Real, J. A. Spin-crossover behavior in cyanide-bridged iron (II)- gold (I) bimetallic 2D Hofmann-like metal- organic frameworks. *Inorganic chemistry* **2008**, *47*, 2552–2561.

(11) Cruddas, J.; Powell, B. J. Structure–property relationships and the mechanisms of multistep transitions in spin crossover materials and frameworks. *Inor. Chem. Front.* **2020**, *7*, 4424–4437.

(12) Cruddas, J.; Powell, B. Spin-state ice in elastically frustrated spin-crossover materials. *Journal of the American Chemical Society* **2019**, *141*, 19790–19799.

(13) Nosé, S. A unified formulation of the constant temperature molecular dynamics methods. *J. Chem. Phys.* **1984**, *81*, 511–519.

(14) Nosé, S. An extension of the canonical ensemble molecular dynamics method. *Molecular Physics* **1986**, *57*, 187–191.

(15) Létard, J.-F. Photomagnetism of iron(ii) spin crossover complexes—the T(LIESST) approach. *J. Mater. Chem.* **2006**, *16*, 2550–2559.

(16) Buron-Le Cointe, M.; Ould Moussa, N.; Trzop, E.; Moréac, A.; Molnar, G.; Toupet, L.; Bousseksou, A.; Létard, J. F.; Matouzenko, G. S. Symmetry breaking and light-induced spin-state trapping in a mononuclear Fe^{II} complex with the two-step thermal conversion. *Phys. Rev. B* **2010**, *82*, 214106.

(17) Enachescu, C.; Linares, J.; Varret, F.; Boukheddaden, K.; Codjovi, E.; Salunke, S. G.; Mukherjee, R. Nonexponential relaxation of the metastable state of the spin-crossover

system $[Fe(L)_2(ClO_4)_2.H_2O$ [L= 2,6-Bis(pyrazole-1-ylmethyl)pyridine]. *Inor. Chem.* **2004**, *43*, 4880–4888.

(18) Mishra, V.; Mukherjee, R.; Linares, J.; Balde, C.; Desplanches, C.; Létard, J.-F.; Collet, E.; Toupet, L.; Castro, M.; Varret, F. temperature-dependent interactions and disorder in the spin-transition compound $[FeII(L)_2][ClO_4]_2.C_7H_8$ through structural, calorimetric, magnetic, photomagnetic, and diffuse reflectance investigations. *Inor. Chem.* **2008**, *47*, 7577–7587.

(19) Kershaw Cook, L. J.; Shepherd, H. J.; Comyn, T. P.; Baldé, C.; Cespedes, O.; Chastanet, G.; Halcrow, M. A. Decoupled spin crossover and structural phase transition in a molecular iron (II) complex. *Chem. - Eur. J.* **2015**, *21*, 4805–4816.

(20) Rodríguez-Velamazán, J. A.; Carbonera, C.; Castro, M.; Palacios, E.; Kitazawa, T.; Létard, J.-F.; Burriel, R. Two-step thermal spin transition and LIESST relaxation of the polymeric spin-crossover compounds $Fe(X{-}py)_2[Ag(CN)_2]_2$ (X=H, 3-methyl, 4-methyl, 3,4-dimethyl, 3-Cl). *Chem. - Eur. J.* **2010**, *16*, 8785–8796.

(21) Money, V. A.; Carbonera, C.; Elhaïk, J.; Halcrow, M. A.; Howard, J. A.; Létard, J.-F. Interplay between kinetically slow thermal spin-crossover and metastable high-spin state relaxation in an iron(II) complex with similar $T_{1/2}$ and T(LIESST). *Chem. - Eur. J.* **2007**, *13*, 5503–5514.

(22) Enachescu, C.; Linares, J.; Codjovi, E.; Boukheddaden, K.; Varret, F. Non-linear behaviour of the spin transition compounds during photo-excitation and relaxation. *J of Optoelectron. Adv. Mater.* **2003**, *5*, 261–266.

(23) Baldé, C.; Bauer, W.; Kaps, E.; Neville, S.; Desplanches, C.; Chastanet, G.; Weber, B.; Létard, J. F. Light-induced excited spin-state properties in 1d iron(ii) chain compounds. *Eur. J. Inorg. Chem.* **2013**, *2013*, 2744–2750.